Angewandte Chemie International Edition

Angewandte International Edition Chemie

How to cite: *Angew. Chem. Int. Ed.* **2026**, 65, e2628759
doi.org/10.1002/anie.2628759

RESEARCH ARTICLE OPEN ACCESS

Two-Dimensional Infrared Spectroscopy Reveals the Presence of a Bridging CO Ligand in Two Catalytic Intermediates of [FeFe] Hydrogenase

Cornelius C. M. Bernitzky[1] | Mathesh Vaithiyanathan[1] | Manon T. Lachmann[2] | Igor V. Sazanovich[3] | Gregory M. Greetham[3] | Patricia Rodríguez-Maciá[2] | James A. Birrell[4] | Marius Horch[1]

[1]Department of Physics, Ultrafast Dynamics in Catalysis, Freie Universität Berlin, Berlin, Germany | [2]School of Chemistry and Leicester Institute for Structural and Chemical Biology, University of Leicester, Leicester, UK | [3]STFC Central Laser Facility, Research Complex at Harwell, Rutherford Appleton Laboratory, Harwell Campus, Didcot, UK | [4]School of Life Sciences, University of Essex, Colchester, UK

Correspondence: James A. Birrell (james.birrell@essex.ac.uk) | Marius Horch (marius.horch@fu-berlin.de)

Received: 19 December 2025 | **Revised:** 19 December 2025 | **Accepted:** 19 March 2026

Keywords:catalytic mechanism| green hydrogen| metalloenzyme| vibrational spectroscopy| organometallic

ABSTRACT

[FeFe] hydrogenases are highly active, reversible enzymes for the interconversion of hydrogen with protons and electrons. Their active site H-cluster consists of a canonical [4Fe-4S] cluster covalently linked to a unique $[2Fe]_H$ centre. Their catalytic mechanism has been studied extensively, but several details remain disputed, and two rival models exist in the literature. One crucial difference between these models is the structure and catalytic relevance of two states named $H_{red}H^+$ and $H_{sred}H^+$. In the first model, these states are catalytic intermediates containing a reduced $[Fe(I)Fe(I)]_H$ centre and a bridging CO ligand (μCO), while in the second model they are inactive states containing an oxidised $[Fe(II)Fe(II)]_H$ site and a bridging hydride ligand (μH^-). The second proposal was initially based on the lack of a prominent absorption peak attributed to a μCO ligand in the infrared (IR) spectra of both states. Here, we provide evidence for the presence of a μCO ligand in the $H_{red}H^+$ and $H_{sred}H^+$ states using two-dimensional (2D) IR spectroscopy, firmly establishing the structure of these states as $[Fe(I)Fe(I)]_H$ with a μCO ligand. The results suggest that these states are catalytically relevant intermediates with crucial implications for understanding hydrogen conversion in nature and designing new synthetic catalysts.

1 | Introduction

Hydrogenases are metalloenzymes that catalyse the reversible production of dihydrogen (H_2) from protons and electrons [1–9]. Of the three classes of hydrogenases ([Fe], [FeFe], [NiFe]), the [FeFe] hydrogenases are reported to be most active and reversible, catalysing H_2 production at rates up to 10 000 s^{-1} and H_2 oxidation rates of over 100 000 s^{-1} [10, 11]. Understanding their catalytic mechanism may enable the design of new synthetic catalysts with comparable activities based on earth-abundant elements.

The [FeFe] hydrogenase's active site H-cluster (Figure 1A) is composed of a canonical [4Fe-4S] cluster ($[4Fe\text{-}4S]_H$) covalently linked through a cysteine thiolate to a unique diiron site ($[2Fe]_H$) [12, 13]. $[2Fe]_H$ is the site of hydrogen formation and oxidation, while $[4Fe\text{-}4S]_H$ acts as an electron storage site. The two Fe ions of $[2Fe]_H$, the proximal (Fe_p) and distal (Fe_d) Fe, named based on their distance from $[4Fe\text{-}4S]_H$, are coordinated by one terminal CO and CN^- ligand each and bridged by two thiolates of a unique 2-azapropane-1,3-dithiolate (ADT) ligand as well as an additional CO (for all structurally characterised

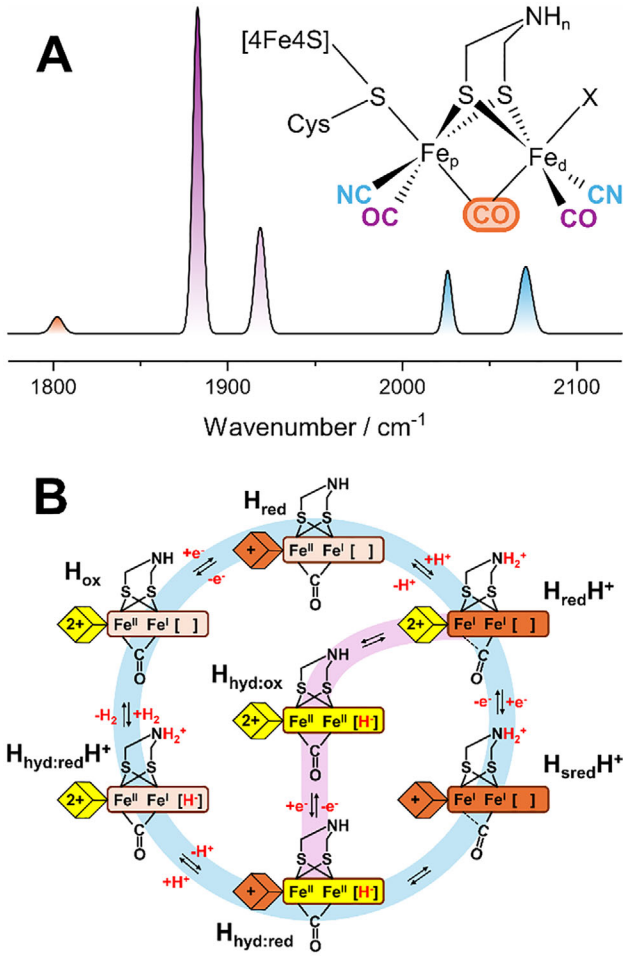

FIGURE 1 | (A) Structure of the active site H-cluster of [FeFe] hydrogenase alongside an idealised FTIR spectrum of the $H_{sred}H^+$ state. "*n*" indicates the possibility that the bridgehead nitrogen can accommodate 1 or 2 H^+. (B) Proposed catalytic cycle in which $H_{red}H^+$ and $H_{sred}H^+$ are integral catalytic intermediates.

states) [14, 15]. The CO and CN^- ligands yield five structurally sensitive and spectrally isolated bond-stretching vibrations that can help identify different states of the H-cluster by infrared (IR) spectroscopy.

Several heatedly debated mechanistic proposals have been formulated [1]. In one model (Figure 1B), the oxidised active state, H_{ox}, consisting of an oxidised $[4Fe\text{-}4S]_H$ ($[4Fe\text{-}4S]_H^{2+}$) and a mixed valence $[2Fe]_H$ ($[Fe_p(II)Fe_d(I)]_H$), is reduced during H_2 production by adding one electron to $[4Fe\text{-}4S]_H$, generating the H_{red} state ($[4Fe\text{-}4S]^+$-$[Fe_p(II)Fe_d(I)]$) [16, 17]. It is debated whether this process is coupled to protonation of $[4Fe\text{-}4S]_H$ (there is also nomenclature discrepancy) [18, 19]. H_{red} is then thought to protonate on the bridgehead nitrogen of the ADT ligand, triggering electron transfer from $[4Fe\text{-}4S]_H$ to $[2Fe]_H$, yielding a $[4Fe\text{-}4S]_H^{2+}$-$[Fe_p(I)Fe_d(I)]H^+$ configuration in the $H_{red}H^+$ state [20, 21]. This frees up $[4Fe\text{-}4S]_H$ for a second reduction, generating the $H_{sred}H^+$ state with a $[4Fe\text{-}4S]_H^+$-$[Fe_p(I)Fe_d(I)]H^+$ configuration [22]. Both $H_{red}H^+$ and $H_{sred}H^+$ are reported to be in tautomeric equilibrium with terminal hydride-bound states called $H_{hyd:ox}$ and $H_{hyd:red}$, respectively, with $[4Fe\text{-}4S]_H^{2+}$-$[Fe_p(II)Fe_d(II)]H^-$ and $[4Fe\text{-}4S]_H^+$-$[Fe_p(II)Fe_d(II)]H^-$ configurations [23]. $H_{hyd:red}$ is just one proton away from forming H_2, and it is hypothesised to protonate at the ADT ligand, followed by electron transfer from $[4Fe\text{-}4S]_H$ to $[2Fe]_H$, proton transfer to the terminal hydride forming H_2, and finally H_2 release [23].

The structure and catalytic importance of $H_{red}H^+$ and $H_{sred}H^+$ remain controversial, especially for extensively studied high-activity model enzymes from *Chlamydomonas reinhardtii* (*Cr*HydA1) and *Desulfovibrio desulfuricans* (*Dd*HydAB). While we and others have proposed the $[Fe(I)Fe(I)]H^+$ configuration with a bridging CO ligand (μCO) [1, 9, 23–25], others have argued that these states are tautomers in which the proton oxidises the Fe ions in $[2Fe]_H$, forming a bridging hydride (μH^-) state, $[4Fe\text{-}4S]_H^{2+}$-$[Fe_p(II)Fe_d(II)]\mu H^-$, as an off-pathway low-activity species (Figure S1) [7, 18, 26, 27]. A central piece of evidence for this μH^- structure is the perceived lack of a μCO peak in the IR spectra of $H_{red}H^+$ and $H_{sred}H^+$ and the appearance of an additional peak in the terminal CO region [16–17, 22]. However, some [FeFe] hydrogenases, specifically sensory enzymes, feature a well-detectable μCO signal in the IR spectra of $H_{red}H^+$ and $H_{sred}H^+$ [25, 28]. The activity of these enzymes is low, though, so that statements about the catalytic involvement of their (super-)reduced states are difficult to make. However, low-temperature IR studies also revealed the appearance of a μCO peak in $H_{red}H^+$ and $H_{sred}H^+$ states of *Cr*HydA1 and *Dd*HydAB [23–25], suggesting that the additional *terminal* CO band is attributable to $H_{hyd:ox}$ and $H_{hyd:red}$ [20]. However, the relevance of these low-temperature studies has been challenged, and the forms of $H_{red}H^+$ and $H_{sred}H^+$ observed at room temperature and low temperature were suggested to be different states [27]. We instead argue that the μCO ligand is difficult to detect at room temperature for most [FeFe] hydrogenases due to peak broadening and an intrinsically low and temperature-dependent extinction coefficient (*vide infra*).

To distinguish between these two scenarios (μCO vs. no μCO) and provide further insight into the structure of these two controversial catalytic intermediates, we decided to use two-dimensional (2D) IR spectroscopy. Briefly, 2D-IR spectroscopy is a nonlinear technique utilising a sequence of ultrashort IR pulses to access multiple vibrational energy levels of a molecule. In the pump-probe implementation, two pump pulses with a controlled time delay typically generate a population in vibrationally excited states, while a probe pulse measures the resulting change in absorbance after a certain waiting time, T_W. Using this approach, detailed insights into the potential energy surface of a molecule, as well as structural and vibrational dynamics, are obtained, as recently demonstrated for both [NiFe] and [FeFe] hydrogenases [29–31, 33]. In particular, 2D-IR spectroscopy reveals anharmonic coupling of different vibrational modes. In this way, peaks observed in the linear IR absorption spectrum can unambiguously be assigned to specific states through cross-peaks in the 2D-IR spectrum. In addition, the nonlinear nature of the experiment facilitates the identification of weak transitions, as associated cross-peaks may gain intensity from coupled bright modes.

2 | Results and Discussion

The 2D-IR spectra of high-activity [FeFe] model hydrogenases from *Chlamydomonas reinhardtii* (*Cr*HydA1) and *Desulfovibrio desulfuricans* (*Dd*HydAB) reduced with sodium dithionite,

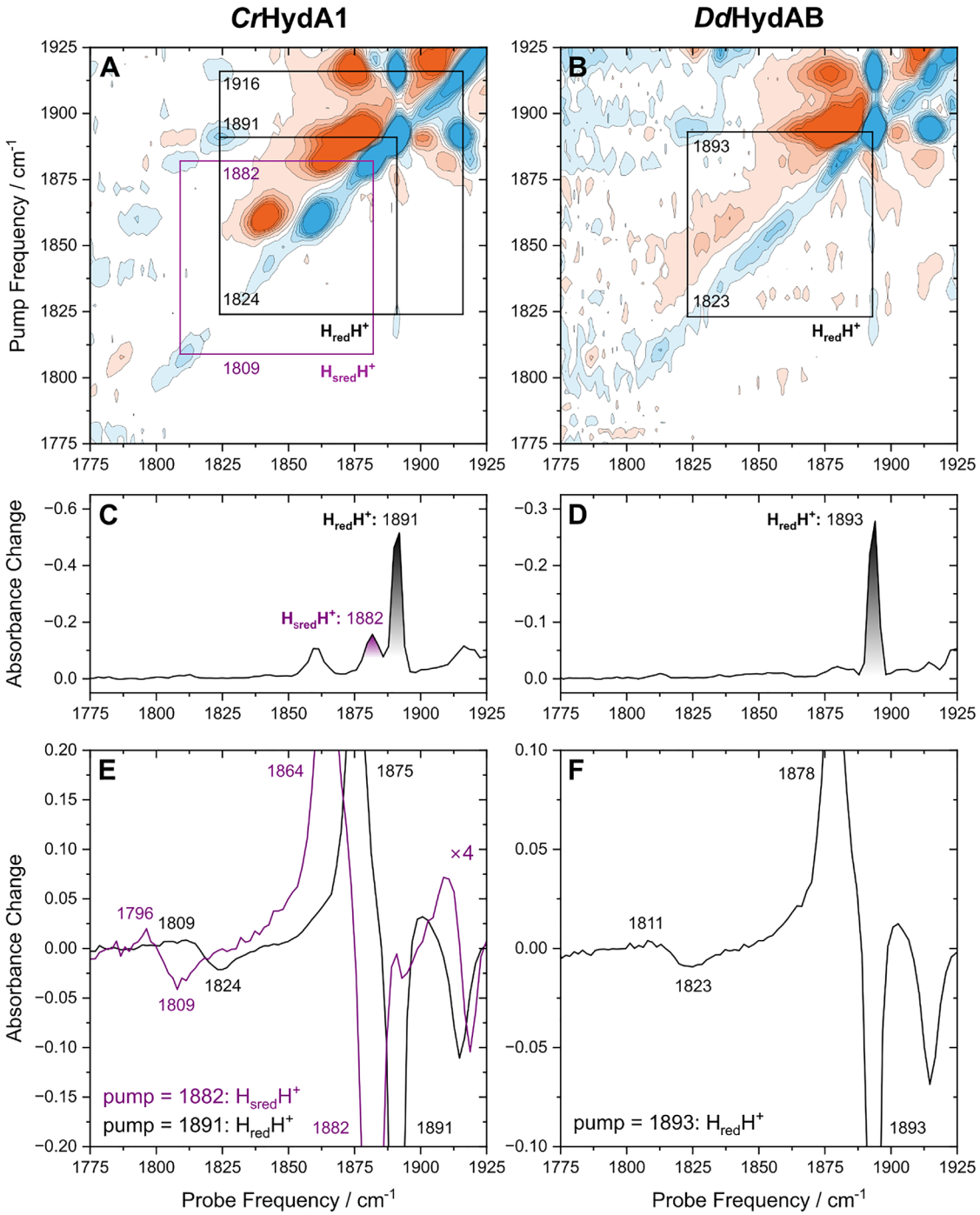

FIGURE 2 | 2D-IR spectra of (A) *Cr*HydA1 and (B) *Dd*HydAB, reduced with sodium dithionite at pH 8. The corresponding sign-inverted diagonal spectra, similar to linear IR spectra, are shown in panels (C) and (D), respectively. Cross-peaks between the most intense tCO mode and the μCO mode are highlighted for $H_{red}H^+$ (black) and $H_{sred}H^+$ (purple) by pump slices through the 2D-IR spectra of (E) *Cr*HydA1 and (F) *Dd*HydAB. Spectra were recorded with perpendicular pump-probe polarisation at $T = 283$ K and $T_W = 0.25$ ps.

recorded with perpendicular polarisation of pump and probe pulses at $T = 283$ K and $T_W = 0.25$ ps, are shown in Figure 2A,B, respectively (spectra recorded with parallel polarization did not yield any extra information). The negative (blue) features on the diagonal (extracted in Figure 2C,D) represent the fundamental transitions of individual vibrational modes that are also seen in the linear IR spectra, while the positive (orange) peaks immediately to the left of them correspond to transitions from an excited state ($v = 1$, $v = 2$, etc.) to higher excited states ($v = 2$, $v = 3$, etc.). Off-diagonal cross-peaks indicate coupling between pairs of vibrational modes. Each of these cross-peaks has a negative (blue) and a positive (red) part. If two modes are coupled, pumping one of them will bleach the shared vibrational ground state. As a consequence, absorption by the second mode is decreased, and a negative signal at the fundamental transition energy is observed, giving a negative cross-peak. In addition, the same pump process generates a population in the vibrationally excited state of the first mode. The second mode can now be

excited from this state, yielding a positive cross-peak, typically at energies slightly lower than the fundamental transition. The latter feature may not be well-observable, though, in some cases, for example, due to a small transition dipole moment of the sequence transition [29, 30, 33]. Diagonal and off-diagonal features are observed for the CO and CN stretching modes of all contributing states, leading to complex signatures in the 2D-IR spectra (see Figures S2–S10 for a detailed assignment). However, both $H_{red}H^+$ and $H_{sred}H^+$ can be clearly identified by their most prominent diagonal signals, which are associated with one of the terminal CO (tCO) stretching modes. These features are observed for $H_{red}H^+$ at 1891 cm^{-1} (*Cr*HydA1) and 1893 cm^{-1} (*Dd*HydAB) and for $H_{sred}H^+$ at 1882 cm^{-1} (*Cr*HydA1). The $H_{sred}H^+$ state is not clearly observed for *Dd*HydAB in these experiments, as the redox potential for its formation is far more negative than for *Cr*HydA1 [16, 32]. Pumping these bright transitions yields cross-peaks between these most intense peaks of $H_{sred}H^+$ and $H_{red}H^+$ and most of the other peaks attributed to them. In addition, clearly observable cross-peaks with bleach contributions at pump/probe frequencies of 1891/1824 cm^{-1} and 1882/1809 cm^{-1} are observed for *Cr*HydA1 and 1893/1823 cm^{-1} for *Dd*HydAB, indicating the presence of a coupled μCO vibration at 1824 cm^{-1} (*Cr*HydA1), 1823 cm^{-1} (*Dd*HydAB) for $H_{red}H^+$, and 1809 cm^{-1} (*Cr*HydA1) for $H_{sred}H^+$. Of note, no prominent diagonal features in the 1800–1830 cm^{-1} region can be detected for $H_{red}H^+$ or $H_{sred}H^+$. While minor contributions of $H_{sred}H^+$ to a diagonal signal observed for *Cr*HydA1 at 1809/1811 cm^{-1} cannot be excluded, this feature mainly corresponded to another state, H_{ox}-CO (see Figure S5), and no such diagonal signal is observed for the $H_{red}H^+$ states in *Cr*HydA1 or *Dd*HydAB, *vide infra*. This finding highlights the difficulty of directly probing these vibrations, as previously observed in linear IR absorption experiments [24]. However, the observation of the identified coupling cross-peaks at early waiting times unambiguously reveals the presence of these vibrations and their affiliation with the assigned $H_{red}H^+$ and $H_{sred}H^+$ states, thereby providing evidence for the presence of a μCO ligand in both states at ambient temperature. Of note, the observed cross-peaks are much more intense than the diagonal transitions since two of the three incoming light-matter interactions (those associated with the pump beam) involve the pronounced transition dipole moment of the bright tCO stretch modes (rather than the weak transition dipole moment of the μCO stretch mode). In addition, the linewidths of the involved transitions do not exceed the off-diagonal anharmonicity. Therefore, positive and negative contributions to the cross-peak do not cancel, in contrast to many other systems where this effect leads to a lowered cross-peak intensity. For *Cr*HydA1, there are also weak cross-peaks at 1808/1885 cm^{-1} and 1822/1891 cm^{-1}, further supporting the assignment of the μCO mode of the $H_{red}H^+$ state. Importantly, no cross-peaks are observed between the most intense peaks identifying $H_{red}H^+$ (1891 and 1893 cm^{-1}) and $H_{sred}H^+$ (1882 cm^{-1}) to any diagonal feature in the 1950–1990 cm^{-1} region (Figure S2). This observation indicates that the peaks observed in this range are not attributed to the $H_{sred}H^+$ and $H_{red}H^+$ states, agreeing with their previous assignment to the tautomeric forms $H_{hyd:red}$ and $H_{hyd:ox}$ (*vide infra*) [23]. Regardless of their origin, we can conclude that no peaks in the 1950–1990 cm^{-1} region are associated with $H_{red}H^+$ and $H_{sred}H^+$.

The features observed in the 2D plots can also be highlighted by taking horizontal "slices" at specific pump frequencies. For *Cr*HydA1, slices at pump frequencies of 1883 cm^{-1} ($H_{sred}H^+$) and 1891 cm^{-1} ($H_{red}H^+$) reveal bleach signals in the μCO region at 1809 and 1824 cm^{-1}, respectively (Figure 2E). Likewise, pumping at 1805 and 1822 cm^{-1} reveals bleach signals at 1882 and 1891 cm^{-1} (Figures S3 and S4). Notably, bleaching is much more pronounced if the bright terminal CO stretch mode is pumped. If these bright modes at 1882 cm^{-1} and 1891 cm^{-1} are pumped, it is also possible to observe bleaches at other frequencies associated with fundamental transitions of $H_{sred}H^+$ and $H_{red}H^+$, respectively (Figures S3 and S4), further supporting the identity of the probed states.

Importantly, no obvious features in the 1950–1990 cm^{-1} region are observed in slices at pump frequencies corresponding to known peaks from $H_{sred}H^+$ or $H_{red}H^+$ neither for *Cr*HydA1 nor *Dd*HydAB (Figures S3, S4, and S10). This further confirms unambiguously that, in contrast to previous suggestions [27], $H_{sred}H^+$ of *Cr*HydA1 and $H_{red}H^+$ of *Cr*HydA1 and *Dd*HydAB do not feature additional terminal CO ligands at ambient temperatures. This finding is fully consistent with the observation of a μCO mode in these states at both ambient and cryogenic conditions [24], that is, $H_{red}H^+$ and $H_{sred}H^+$ have the same structure at all investigated temperatures. The unambiguous observation of a μCO ligand negates the possibility of these states containing a μH^- ligand. This implies minimal structural reorganisation during the formation of these states. We conclude, therefore, that $H_{red}H^+$ and $H_{sred}H^+$ are catalytic intermediates that form part of the main catalytic cycle for producing and oxidising hydrogen. They both contain a fully reduced diiron site that is capable of tautomerising to terminal hydride-containing states, $H_{hyd:ox}$ and $H_{hyd:red}$, which also suggests protonation of the amine bridgehead [23]. So far, $H_{hyd:ox}$ and $H_{hyd:red}$ have only been substantially populated under cryogenic illumination of $H_{red}H^+$ and $H_{sred}H^+$ [23]. However, the previous observation of IR peaks in the 1950–1990 cm^{-1} region may indicate the presence of a proportion of these states at room temperature [23, 24]. We attempted to quantify the proportion of the hydride-tautomers in room-temperature linear IR spectra (Figure S11). We also investigated the influence of buffer composition, pH and salt concentration and found little effect (Figures S12 and S13; Table S2).

The 2D-IR cross peaks discussed above result from anharmonic coupling between tCO modes and the μCO mode. Therefore, they are observed from the earliest waiting times on, providing unambiguous proof that both types of modes correspond to the same state, that is, $H_{red}H^+$ and $H_{sred}H^+$. Apart from anharmonic coupling, cross peaks in 2D-IR spectra can also arise from energy transfer between vibrational modes. In that case, the cross peaks grow into the spectrum as a function of the waiting time, T_W. Notably, the separation of positive and negative parts in energy-transfer cross peaks does *not* reflect the *off-diagonal* anharmonicity, i.e. the coupling between the two modes. Instead, the separation reflects the *diagonal* anharmonicity of the mode that has *not* been pumped, reflecting population transfer from the pumped mode. As a consequence, cross peaks from energy transfer provide additional insights into dark modes that do not produce noticeable diagonal signals. Focusing on data from *Cr*HydA1 and the $H_{red}H^+$ state, which showed higher overall signal intensities (*vide supra*), we therefore recorded 2D-IR spectra at a longer waiting time of $T_W = 3$ ps (Figure 3). Pumping the brightest tCO mode of $H_{red}H^+$, clear cross peaks can be

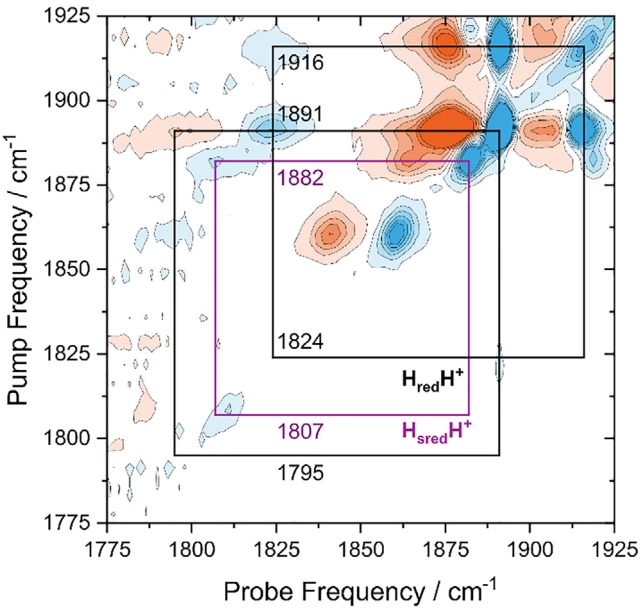

FIGURE 3 | 2D-IR spectrum of *Cr*HydA1, reduced with sodium dithionite at pH 8. The spectrum was recorded with perpendicular pump-probe polarisation at $T = 283$ K and $T_W = 3$ ps. Another dataset with a higher population of $H_{sred}H^+$ is shown in Figure S14. Note that the frequency of the positive cross-peak of $H_{red}H^+$ (1795 cm^{-1}) is likely underestimated, due to strong broadening (see Figure S14). Likewise, the negative cross peak of $H_{sred}H+$ (1807 cm^{-1}) is lower in frequency than observed at $T_W = 0.25$ ps (1809 cm^{-1}, see Figure 2A,E). The value obtained at $T_W = 3$ ps may be more reliable (see Figure S14), but, for the sake of consistency, we refer to the value initially obtained at $T_W = 0.25$ ps throughout the manuscript.

identified that link the most prominent tCO signal at 1891 cm^{-1} to a dark transition at 1824 cm^{-1}. Consistent with the above findings from early waiting times ($T_W = 0.25$ ps), we assign this dark transition to the μCO mode of $H_{red}H^+$. Further proof for this assignment comes from inspecting the separation between positive and negative parts of the cross peaks. While the coupling cross peaks discussed above show a separation of 10–15 cm^{-1} (Figure 2E), the separation in the energy-transfer cross peak is significantly larger, on the order of ≥ 25 cm^{-1}. This value reflects the diagonal anharmonicity of the dark transitions at 1824 cm^{-1}, which can be extracted since its first vibrationally excited state has been populated via energy transfer from the pumped bright mode. The obtained value matches general expectations for a bond-localized stretching vibration of a metal-bound CO ligand [29, 30, 33–38] and, more specifically, the value observed for the μCO mode of [FeFe] hydrogenase [31]. Similar features can also be observed for $H_{sred}H^+$ in individual datasets (Figure S14), but the signals are typically less pronounced due to a lower population of this intermediate. In total, the dark transition at 1824 and 1809 cm^{-1}reflect μCO modes, as evident from observed diagonal and off-diagonal anharmonicities (Figure S15) as well as low fundamental frequencies, thereby proving the presence of a bridging CO ligand in both $H_{red}H^+$ and $H_{sred}H^+$.

An interesting observation is that the μCO mode in $H_{red}H^+$ and $H_{sred}H^+$ appears at a higher frequency at room temperature (1824 and 1809 cm^{-1}) than at cryogenic temperatures (1817 and 1801 cm^{-1}) [23, 24]. The 7–8 cm^{-1} difference may be due to differences in the vibrationally averaged structure (varying degrees of thermally excited low-frequency modes), which seems to yield a more bridging configuration (with low μCO frequency) at cryogenic temperatures and a semi-bridging one (with higher μCO frequency) at room temperature. A plot of peak position vs. temperature for the μCO mode in $H_{sred}H^+$ of *Cr*HydA1 shows a linear trend between 40 and 200 K (Figure S16). It is also interesting that the μCO modes in $H_{red}H^+$ and $H_{sred}H^+$, in which $[2Fe]_H$ has acquired an extra reducing equivalent, are not downshifted with respect to the μCO peak observed in states with an Fe(II)Fe(I) ground state, that is, H_{ox} (1803 cm^{-1} for *Cr*HydA1 [21]; 1802 cm^{-1} for *Dd*HydAB [32]) and H_{red} (1791 cm^{-1} for *Cr*HydA1 [21]; 1792 cm^{-1} for *Dd*HydAB [32]). Meanwhile, the main terminal CO ligands are downshifted by about 50 cm^{-1} (1883/1891 cm^{-1} in $H_{sred}H^+/H_{red}H^+$ vs. 1933/1939 cm^{-1} in H_{red}/H_{ox} for *Cr*HydA1 [21] and 1883/1893 cm^{-1} in $H_{sred}H^+/H_{red}H^+$ vs. 1934/1940 cm^{-1} in H_{red}/H_{ox} for *Dd*HydA1 [32]). This suggests that the μCO ligand becomes less bridging and more terminal in $H_{sred}H^+$ and $H_{red}H^+$ compared with H_{ox}/H_{red}, which counteracts the red shift caused by adding an additional electron onto the $[2Fe]_H$ site (Figure 4). Additional electron density on the Fe ions is thought to be donated into the π^* antibonding molecular orbitals of the CO (and CN^-) ligands. If the bridging CO partially shifts toward Fe_d in the $H_{red}H^+$ and $H_{sred}H^+$ states, due to significant population of the d_z^2 orbital and the pronounced *trans* influence of the cysteine on Fe_p, there will be reduced π backdonation from Fe_p, which will compensate for the increased π backdonation due to the extra electron on $[2Fe]_H$.

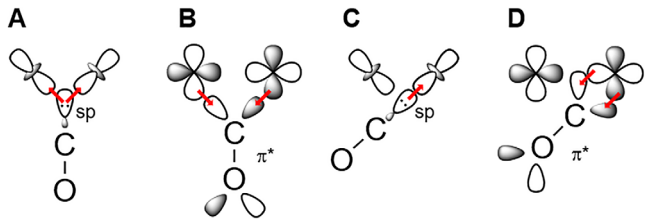

FIGURE 4 | Scheme showing the metal-ligand binding in bridging (A, B) and terminal (C, D) CO arrangements. The filled CO σ molecular orbital donates electron density into the (partly) empty metal e_g *d*-orbitals ($d_x^2{}_{-y}^2$ or d_z^2, A and C). The filled metal t_{2g} d-orbitals (d_{xy}, d_{xz}, or d_{yz}) donate electron density into the empty CO π^* molecular orbital. The orientation of the CO ligand that is favoured will depend on the orbital overlap and occupancy of the metal e_g *d*-orbitals. In the low-spin Fe(II) state, both e_g orbitals are empty; in the low-spin Fe(I) state, there is one electron in one of the e_g orbitals, and the other is empty.

3 | Conclusion

In conclusion, we discount that $H_{red}H^+$ and $H_{sred}H^+$ are bridging-hydride-containing off-pathway states (assumed to be low activity). Instead, these states were identified as CO-bridged intermediates that form a critical part of the catalytic cycle, allowing the H_{ox} resting state to be transformed to tautomeric hydride states with minimal structural reorganisation, thereby facilitating H_2 evolution at unrivalled rates. The central involvement of these reduced states also implies a mechanism where protonation of the ADT bridgehead atom and electron accumulation on the

$[2Fe]_H$ center are intimately coupled. In particular, the more reduced $H_{hyd:red}$ hydride state, a tautomer of $H_{sred}H^+$, is likely to become protonated on the bridgehead ADT nitrogen, yielding a $H_{hyd:red}H^+$-type state. We speculate that this step involves electron transfer from $[4Fe\text{-}4S]_H$ to $[2Fe]_H$, yielding an H_{ox}-like electronic ground state. Such a state would have a $[2Fe]_H$ cluster that is too electron-rich, thereby weakening the Fe–H^- bond and favouring protonation of the hydride to yield H_2. Subsequent studies using further ultrafast IR techniques coupled to isotope-exchange studies on protonation and hydride-formation steps could provide evidence for this proposed mechanism, specifically the catalytic competence of the $H_{red}H^+$ and $H_{sred}H^+$ states, and may yield additional insight into the catalytic cycle of [FeFe] hydrogenases.

Acknowledgements

This work was funded by the Deutsche Forschungsgemeinschaft (DFG, German Research Foundation) under Germany's Excellence Strategy – EXC 2008 – 390540038, UniSysCat (Unifying Systems in Catalysis). CCMB and MH are grateful for financial support by the Einstein Foundation Berlin. PRM thanks the Royal Society (Grant Number. RGS\R1\231433), the Royal Society of Chemistry (Grant Number. R23-6753486967) and the University of Leicester for funding. MTL is financially supported by a Future 50 Scholarship from the University of Leicester. JAB acknowledges funding from the Royal Society (Grant Number. RG\R2\232336), the Royal Society of Chemistry (Grant Number. R22-2594924113), and the University of Essex. The authors thank the STFC for funding access to the ULTRA laser system at the STFC Central Laser Facility (23130006). The research leading to these results has received funding from LASERLAB-EUROPE (grant agreement no. 871124, European Union's Horizon 2020 research and innovation programme). The authors kindly thank Marta Szynkiewicz, Dr. Paul M. Donaldson, Dr. Ian P. Clark, and Dr. Partha Malakar from the STFC-CLF for invaluable support prior to and during measurements.

Conflicts of Interest

The authors declare no conflicts of interest.

Data Availability Statement

The data that supports the findings of this study are available from the corresponding author upon reasonable request.

References

1. J. A. Birrell, P. Rodríguez-Maciá, E. J. Reijerse, M. A. Martini, and W. Lubitz, "The Catalytic Cycle of [FeFe] Hydrogenase: A Tale of Two Sites," *Coordination Chemistry Reviews* 449 (2021): 214191, https://doi.org/10.1016/j.ccr.2021.214191.

2. H. Ji, L. Wan, Y. Gao, et al., "Hydrogenase as the Basis for Green Hydrogen Production and Utilization," *Journal of Energy Chemistry* 85 (2023): 348–362, https://doi.org/10.1016/j.jechem.2023.06.018.

3. J. T. Kleinhaus, F. Wittkamp, S. Yadav, D. Siegmund, and U.-P. Apfel, "[FeFe]-Hydrogenases: Maturation and Reactivity of Enzymatic Systems and Overview of Biomimetic Models," *Chemical Society Reviews* 50 (2021): 1668–1784, https://doi.org/10.1039/D0CS01089H.

4. W. Lubitz, H. Ogata, O. Rüdiger, and E. Reijerse, "Hydrogenases," *Chemical Reviews* 114 (2014): 4081–4148, https://doi.org/10.1021/cr4005814.

5. S. Morra, "Fantastic [FeFe]-hydrogenases and Where to Find Them," *Frontiers in Microbiology* 13 (2022): 853626, https://doi.org/10.3389/fmicb.2022.853626.

6. P. M. Vignais and B. Billoud, "Occurrence, Classification, and Biological Function of Hydrogenases: An Overview," *Chemical Reviews* 107 (2007): 4206–4272, https://doi.org/10.1021/cr050196r.

7. M. Haumann and S. T. Stripp, "The Molecular Proceedings of Biological Hydrogen Turnover," *Accounts of Chemical Research* 51 (2018): 1755–1763, https://doi.org/10.1021/acs.accounts.8b00109.

8. H. Land, M. Senger, G. Berggren, and S. T. Stripp, "Current State of [FeFe]-Hydrogenase Research: Biodiversity and Spectroscopic Investigations," *ACS Catalysis* 10 (2020): 7069–7086, https://doi.org/10.1021/acscatal.0c01614.

9. M. T. Lachmann, Z. Duan, P. Rodríguez-Maciá, and J. A. Birrell, "The Missing Pieces in the Catalytic Cycle of [FeFe] Hydrogenases," *Chemical Science* 15 (2024): 14062–14080, https://doi.org/10.1039/D4SC04041D.

10. B. R. Glick, W. G. Martin, and S. M. Martin, "Purification and Properties of the Periplasmic Hydrogenase From *Desulfovibrio desulfuricans*," *Canadian Journal of Microbiology* 26 (1980): 1214–1223, https://doi.org/10.1139/m80-203.

11. E. C. Hatchikian, N. Forget, V. M. Fernandez, R. Williams, and R. Cammack, "Further Characterization of the [Fe]-Hydrogenase From Desulfovibrio Desulfuricans ATCC 7757," *European Journal of Biochemistry* 209 (1992): 357–365, https://doi.org/10.1111/j.1432-1033.1992.tb17297.x.

12. Y. Nicolet, C. Piras, P. Legrand, C. E. Hatchikian, and J. C. Fontecilla-Camps, "Desulfovibrio Desulfuricans Iron Hydrogenase: The Structure Shows Unusual Coordination to an Active Site Fe Binuclear Center," *Structure (London, England)* 7 (1999): 13–23, https://doi.org/10.1016/S0969-2126(99)80005-7.

13. J. W. Peters, "X-Ray Crystal Structure of the Fe-Only Hydrogenase (CpI) From Clostridium Pasteurianum to 1.8 Angstrom Resolution," *Science* 282 (1998): 1853–1858, https://doi.org/10.1126/science.282.5395.1853.

14. A. Silakov, B. Wenk, E. Reijerse, and W. Lubitz, "^{14}N HYSCORE Investigation of the H-Cluster of [FeFe] Hydrogenase: Evidence for a Nitrogen in the Dithiol Bridge," *Physical Chemistry Chemical Physics* 11 (2009): 6592, https://doi.org/10.1039/b905841a.

15. G. Berggren, A. Adamska, C. Lambertz, et al., "Biomimetic Assembly and Activation of [FeFe]-Hydrogenases," *Nature* 499 (2013): 66–69, https://doi.org/10.1038/nature12239.

16. W. Roseboom, A. L. De Lacey, V. M. Fernandez, E. C. Hatchikian, and S. P. J. Albracht, "The Active Site of the [FeFe]-hydrogenase From *Desulfovibrio desulfuricans*. II. Redox Properties, Light Sensitivity and CO-ligand Exchange as Observed by Infrared Spectroscopy," *Journal of Biological Inorganic Chemistry* 11 (2006): 102–118, https://doi.org/10.1007/s00775-005-0040-2.

17. A. Silakov, C. Kamp, E. Reijerse, T. Happe, and W. Lubitz, "Spectroelectrochemical Characterization of the Active Site of the [FeFe] Hydrogenase HydA1 From *Chlamydomonas reinhardtii*," *Biochemistry* 48 (2009): 7780–7786, https://doi.org/10.1021/bi9009105.

18. M. Senger, K. Laun, F. Wittkamp, et al., "Proton-Coupled Reduction of the Catalytic [4Fe-4S] Cluster in [FeFe]-Hydrogenases," *Angewandte Chemie International Edition* 56 (2017): 16503–16506, https://doi.org/10.1002/anie.201709910.

19. P. Rodríguez-Maciá, N. Breuer, S. DeBeer, and J. A. Birrell, "Insight Into the Redox Behavior of the [4Fe–4S] Subcluster in [FeFe] Hydrogenases," *ACS Catalysis* 10 (2020): 13084–13095.

20. S. Katz, J. Noth, M. Horch, et al., "Vibrational Spectroscopy Reveals the Initial Steps of Biological Hydrogen Evolution," *Chemical Science* 7 (2016): 6746–6752, https://doi.org/10.1039/C6SC01098A.

21. C. Sommer, A. Adamska-Venkatesh, K. Pawlak, et al., "Proton Coupled Electronic Rearrangement Within the H-Cluster as an Essential Step in the Catalytic Cycle of [FeFe] Hydrogenases," *Journal of the American Chemical Society* 139 (2017): 1440–1443, https://doi.org/10.1021/jacs.6b12636.

22. A. Adamska, A. Silakov, C. Lambertz, et al., "Identification and Characterization of the 'Super-Reduced' State of the H-Cluster in [FeFe] Hydrogenase: A New Building Block for the Catalytic Cycle?" *Angewandte Chemie International Edition* 51 (2012): 11458–11462, https://doi.org/10.1002/anie.201204800.

23. C. Lorent, S. Katz, J. Duan, et al., "Shedding Light on Proton and Electron Dynamics in [FeFe] Hydrogenases," *Journal of the American Chemical Society* 142 (2020): 5493–5497, https://doi.org/10.1021/jacs.9b13075.

24. J. A. Birrell, V. Pelmenschikov, N. Mishra, et al., "Spectroscopic and Computational Evidence That [FeFe] Hydrogenases Operate Exclusively With CO-Bridged Intermediates," *Journal of the American Chemical Society* 142 (2020): 222–232, https://doi.org/10.1021/jacs.9b09745.

25. M. W. Ratzloff, J. H. Artz, D. W. Mulder, R. T. Collins, T. E. Furtak, and P. W. King, "CO-Bridged H-Cluster Intermediates in the Catalytic Mechanism of [FeFe]-Hydrogenase *Ca*I," *Journal of the American Chemical Society* 140 (2018): 7623–7628, https://doi.org/10.1021/jacs.8b03072.

26. M. Senger, S. Mebs, J. Duan, et al., "Protonation/Reduction Dynamics at the [4Fe–4S] Cluster of the Hydrogen-Forming Cofactor in [FeFe]-Hydrogenases," *Physical Chemistry Chemical Physics* 20 (2018): 3128–3140, https://doi.org/10.1039/C7CP04757F.

27. S. T. Stripp, S. Mebs, and M. Haumann, "Temperature Dependence of Structural Dynamics at the Catalytic Cofactor of [FeFe]-Hydrogenase," *Inorganic Chemistry* 59 (2020): 16474–16488, https://doi.org/10.1021/acs.inorgchem.0c02316.

28. N. Chongdar, J. A. Birrell, K. Pawlak, et al., "Unique Spectroscopic Properties of the H-cluster in a Putative Sensory [FeFe] Hydrogenase," *Journal of the American Chemical Society* 140 (2018): 1057–1068, https://doi.org/10.1021/jacs.7b11287.

29. M. Horch, J. Schoknecht, S. L. D. Wrathall, G. M. Greetham, O. Lenz, and N. T. Hunt, "Understanding the Structure and Dynamics of Hydrogenases by Ultrafast and Two-Dimensional Infrared Spectroscopy," *Chemical Science* 10 (2019): 8981–8989, https://doi.org/10.1039/C9SC02851J.

30. S. L. D. Wrathall, B. Procacci, M. Horch, et al., "Ultrafast 2D-IR Spectroscopy of [NiFe] Hydrogenase From *E. coli* Reveals the Role of the Protein Scaffold in Controlling the Active Site Environment," *Physical Chemistry Chemical Physics* 24 (2022): 24767–24783, https://doi.org/10.1039/D2CP04188J.

31. C. C. M. Bernitzky, Y. Rippers, D. Poire, et al., "Two-dimensional Infrared Spectroscopy as a Tool to Reveal the Vibrational and Molecular Structure of [FeFe] Hydrogenases," *Chemical Science* 16 (2025): 10957–10969, https://doi.org/10.1039/D5SC01811K.

32. P. Rodríguez-Maciá, K. Pawlak, O. Rüdiger, E. J. Reijerse, W. Lubitz, and J. A. Birrell, "Intercluster Redox Coupling Influences Protonation at the H-Cluster in [FeFe] Hydrogenases," *Journal of the American Chemical Society* 139 (2017): 15122–15134.

33. C. J. Kulka-Peschke, A.-C. Schulz, C. Lorent, et al., "Reversible Glutamate Coordination to High-Valent Nickel Protects the Active Site of a [NiFe] Hydrogenase From Oxygen," *Journal of the American Chemical Society* 144 (37) (2022): 17022–17032, https://doi.org/10.1021/jacs.2c06400.

34. B. Procacci, S. L. D. Wrathall, A. L. Farmer, et al., "Understanding the [NiFe] Hydrogenase Active Site Environment Through Ultrafast Infrared and 2D-IR Spectroscopy of the Subsite Analogue $K[CpFe(CO)(CN)_2]$ in Polar and Protic Solvents," *Journal of Physical Chemistry B* 128 (2024): 1461–1472, https://doi.org/10.1021/acs.jpcb.3c07965.

35. J. C. Owrutsky, M. Li, B. Locke, and R. M. Hochstrasser, "Vibrational Relaxation of the CO Stretch Vibration in Hemoglobin-CO, Myoglobin-CO, and Protoheme-CO," *Journal of Physical Chemistry* 99 (1995): 4842–4846, https://doi.org/10.1021/j100013a064.

36. C. Falvo, L. Daniault, T. Vieille, et al., "Ultrafast Dynamics of Carboxy-Hemoglobin: Two-dimensional Infrared Spectroscopy Experiments and Simulations," *Journal of Physical Chemistry Letters* 6 (2015): 2216–2222, https://doi.org/10.1021/acs.jpclett.5b00811.

37. K. A. Merchant, W. G. Noid, R. Akiyama, et al., "Myoglobin-CO Substate Structures and Dynamics: Multidimensional Vibrational Echoes and Molecular Dynamics Simulations," *Journal of the American Chemical Society* 125 (2003): 13804–13818, https://doi.org/10.1021/ja035654x.

38. I. J. Finkelstein, B. L. McClain, and M. D. Fayer, "Fifth-order Contributions to Ultrafast Spectrally Resolved Vibrational Echoes: Heme-CO Proteins," *Journal of Chemical Physics* 121 (2004): 877–885, https://doi.org/10.1063/1.1758940.

39. J. A. Birrell, K. Wrede, K. Pawlak, et al., "Artificial Maturation of the Highly Active Heterodimeric [FeFe] Hydrogenase from *Desulfovibrio desulfuricans* ATCC 7757," *Israel Journal of Chemistry* 56 (2016): 852–863, https://doi.org/10.1002/ijch.201600035.

40. J. Esselborn, C. Lambertz, A. Adamska-Venkatesh, et al., "Spontaneous Activation of [FeFe]-Hydrogenases by an Inorganic [2Fe] Active Site Mimic," *Nature Chemical Biology* 9 (2013): 607–609, https://doi.org/10.1038/nchembio.1311.

41. L. P. DeFlores, R. A. Nicodemus, and A. Tokmakoff, "Two-dimensional Fourier Transform Spectroscopy in the Pump-Probe Geometry," *Optics Letters* 32 (2007): 2966–2968, https://doi.org/10.1364/OL.32.002966.

42. S.-H. Shim, D. B. Strasfeld, Y. L. Ling, and M. T. Zanni, "Automated 2D IR Spectroscopy Using a Mid-IR Pulse Shaper and Application of this Technology to the Human Islet Amyloid Polypeptide," *Proceedings of the National Academy of Sciences* 104 (2007): 14197–14202, https://doi.org/10.1073/pnas.0700804104.

43. S.-H. Shim and M. T. Zanni, "How to Turn Your Pump–Probe Instrument into a Multidimensional Spectrometer: 2D IR and Vis Spectroscopies via Pulse Shaping," *Physical Chemistry Chemical Physics*11 (2009): 748–761, https://doi.org/10.1039/B813817F.

44. G. M. Greetham, P. Burgos, Q. Cao, et al., "Ultra: A Unique Instrument for Time-Resolved Spectroscopy," *Applied Spectroscopy* 64 (2010): 1311–1319, https://doi.org/10.1366/000370210793561673.

45. M. Lorenzi, J. Gellett, A. Zamader, et al., "Investigating the Role of the Strong Field Ligands in [FeFe] Hydrogenase: Spectroscopic and Functional Characterization of a Semi-Synthetic Mono-cyanide Active Site," *Chemical Science* 13 (2022): 11058–11064, https://doi.org/10.1039/D2SC02271K.

46. V. Fourmond, "QSoas: A Versatile Software for Data Analysis," *Analytical Chemistry* 88 (2016): 5050–5052, https://doi.org/10.1021/acs.analchem.6b00224.

Supporting Information

Additional supporting information can be found online in the Supporting Information section.

The authors have cited additional references within the Supporting Information [39–46].